ARTHRITIS & RHEUMATISM
Vol. 63, No. 10, October 2011, pp 3126–3135
DOI 10.1002/art.30500

Changes in Rab3D Expression and Distribution in the Acini of Sjögren's Syndrome Patients Are Associated With Loss of Cell Polarity and Secretory Dysfunction

Verónica Bahamondes,[1] Amelina Albornoz,[1] Sergio Aguilera,[2] Cecilia Alliende,[1] Claudio Molina,[3] Isabel Castro,[1] Ulises Urzúa,[1] Andrew F. G. Quest,[1] María-José Barrera,[1] Sergio González,[4] Marianela Sánchez,[1] Steffen Härtel,[1] Marcela Hermoso,[1] Cecilia Leyton,[1] and María-Julieta González[1]

Objective. **Oral and ocular dryness are frequent and serious symptoms of Sjögren's syndrome (SS) that reflect problems in secretion due to glandular dysfunction. Exocytosis, an important process in the secretory pathway, requires the participation of Rab family GTPases. This study was undertaken to analyze the expression and localization of Rab3D and Rab8A and to examine their correlation with acinar cell polarity and glandular secretory function.**

Methods. **Nineteen patients with SS and 17 controls were evaluated. Levels of Rab3D and Rab8A messenger RNA (mRNA) and protein were determined by real-time polymerase chain reaction and Western blotting. Subcellular localization of proteins was determined by indirect immunofluorescence analysis.**

Results. **In patients with SS, total Rab3D protein levels decreased significantly, while mRNA levels remained unchanged. For Rab8A, no changes in either mRNA or protein levels were detected. In serous acini of labial salivary glands from patients with SS, the following 4 patterns of Rab3D staining were distinguishable: severely decreased, distribution throughout the cytoplasm, distribution throughout the cytoplasm combined with loss of nuclear polarity, and normal apical localization. Basal localization of Rab8A was not modified. Rab3D changes were accompanied by apicobasolateral redistribution of ezrin, loss of nuclear polarity, thicker Golgi stacks, and mucin 7 accumulation in the cytoplasm. Finally, low Rab3D protein levels correlated with alterations in scintigraphy measurements.**

Conclusion. **Our findings indicate that Rab3D regulates the exocytosis of many components critical for the maintenance of oral physiology. Hence, the changes observed in Rab3D expression and distribution are likely to contribute to the decrease in or loss of saliva components (i.e., mucins), which may explain the variety of oral and ocular symptoms associated with SS.**

Apoptosis and cytotoxic cell death have been implicated in the loss of glandular tissue and in glandular dysfunction in patients with Sjögren's syndrome (SS) (1–3). Alternatively, a novel nonapoptotic model has been put forward in which alterations in immune responses are associated with changes in the secretory process of acinar cells (4). A fraction of SS patients with markedly diminished or absent saliva output have large areas of apparently normal salivary glandular tissue, but display reduced sensitivity to muscarinic stimulation (4–6). Studies in a murine model of SS have focused exclusively on water output as the final product of stimulus–secretion coupling (4). Water channels (i.e.,

Supported by FONDECYT grant 1080006 (to Drs. Aguilera and Molina and Ms M.-J. González), FONDECYT grant 1090246 (to Dr. Härtel), and FONDECYT-FONDAP grant 15010006 (to Dr. Quest), and by a CONICYT PhD fellowship (to Ms Barrera).

[1]Verónica Bahamondes, BSc, Amelina Albornoz, BSc, Cecilia Alliende, BSc, Isabel Castro, MSc, Ulises Urzúa, PhD, Andrew F. G. Quest, PhD, María-José Barrera, BSc, Marianela Sánchez, BSc, Steffen Härtel, PhD, Marcela Hermoso, PhD, Cecilia Leyton, MSc, María-Julieta González, MSc: University of Chile, Santiago, Chile; [2]Sergio Aguilera, MD: Indisa Clinic, Santiago, Chile; [3]Claudio Molina, DDS, MSc: Mayor University, Santiago, Chile; [4]Sergio González, DDS, MSc: Mayor University and San Sebastián University, Santiago, Chile.

Dr. Aguilera and Ms M.-J. González contributed equally to this work.

Address correspondence to María-Julieta González, MSc, Instituto de Ciencias Biomédicas, Facultad de Medicina, Universidad de Chile, Casilla 70061, Santiago 7, Chile. E-mail: jgonzale@med.uchile.cl.

Submitted for publication February 1, 2011; accepted in revised form June 9, 2011.

aquaporin 5) and anion channels (i.e., Cl^-) are involved in the release of water and electrolytes from the apical pole of acinar cells. Cation channels (i.e., Na^+) mediate paracellular flux (7). The present study focused on analyzing the proteins that participate in secretory granule trafficking in salivary glands.

Classically, the xerostomia observed in SS patients has been associated exclusively with reduced quantities of water, rather than altered properties of other saliva components, including diverse proteins, glycoproteins, and mucins (4). Dramatic decreases in mucin 5B (MUC5B) sulfation have been observed in the mucous acini of labial salivary glands (LSGs) from SS patients, and these changes are unrelated to changes in saliva volume (8). Importantly, sulfated and sialylated oligosaccharides are required in MUC5B to bind water essential for moisturizing the oral mucosa (9). These observations suggest that alterations in the secretory pathway of acinar cells, particularly at the level of the Golgi complex, the site where mucins undergo posttranslational processing including sulfation, may be relevant to SS development.

Correct acinar cell polarity is fundamental to maintaining the basolateral-apical directionality of the secretory route. Both tight junctions and acinar cell–extracellular matrix interactions play key roles in this respect. Important changes in the polarity of LSG acinar cells from SS patients have been reported recently (7,10,11). LSG acini from SS patients display alterations in structural components of the acinar apical pole, including a dilated lumen, loss of microvilli, and structural changes in the remaining microvilli (10). Ezrin and the actin cytoskeleton are well-established microvilli organizers. Accordingly, disrupted microvilli structures and apicobasolateral ezrin delocalization are consistently observed in the epithelial cells of LSGs from SS patients (11). Also, changes in staining intensity and distribution of actin have been reported (11). A loss of ezrin observed at the apical pole can be expected to alter interactions between the actin cytoskeleton and the apical plasma membrane and thereby contribute to impairment of the secretory process in SS patients (11).

Exocytosis of granule contents involves highly controlled targeting, docking, and fusion of mature secretory granules with the apical plasma membrane. Interestingly, larger pleomorphic secretory granules have consistently been observed in LSGs from SS patients compared to those from control subjects, suggesting possible fusion events in SS (10). Taken together, these data are indicative of modifications in the secretory machinery of LSG epithelial cells in SS patients.

Exocytosis is a complex process that depends on the functionality of many proteins. In this study, we were particularly interested in evaluating the role of small GTPases of the Rab3 family. Rab proteins are members of the Ras-related small G protein family that participate in various steps of intracellular vesicle trafficking, including exocytosis, where they ensure fidelity of recognition between vesicles and target membranes by recruiting specific effectors required for membrane fusion and cargo delivery (12,13). The Rab3 protein subfamily, composed of 4 isoforms (A–D) expressed in different tissue types, has been postulated to participate in a final step that facilitates exocytosis (14). In exocrine glands, such as the pancreas, parotid glands, and lacrimal glands, Rab3D represents the predominant isoform (15). However, the precise function of Rab3D in acinar secretion remains unclear, although it is known to associate with mature secretory granules localized at the apical pole of acinar cells and its abundance there decreases with apical exocytosis (16,17). Additionally, overexpression of wild-type Rab3D enhances, while dominant-negative forms reduce, amylase secretion in pancreatic acini, suggesting that Rab3D participates directly in acinar exocytosis (18). Interestingly, da Costa et al have reported that secretory vesicles in lacrimal glands from male nonobese diabetic (NOD) mice, an animal model of SS, exhibit profound morphologic changes, including an increase in the size of secretory granules that are linked to Rab3D alterations (19).

To date, Rab3D expression and localization have not been compared with other cell polarity markers of the secretory pathway in salivary glands from SS patients. Changes in acinar cell polarity are likely to affect the localization of both secretory granules and Rab3D, which in turn may contribute to alterations in functional parameters. In this study, Rab3D messenger RNA (mRNA) and protein levels as well as localization were compared with those of Rab8A, a marker of basal vesicle membranes, and other cell polarity markers. These molecular and morphologic data were correlated with functional parameters.

PATIENTS AND METHODS

Patients with primary SS and controls. All subjects signed an informed consent form following guidelines established by the Ethics Committee of the Faculty of Medicine, University of Chile. The study group included 36 nonsmokers with good oral hygiene who had presented to their physician with the symptoms dry eyes and dry mouth during the previous 3 months. Nineteen individuals were diagnosed as having primary SS according to the American–European Consensus

Table 1. Demographic, serologic, and histologic characteristics of the controls and patients with SS*

	Controls (n = 17)	SS patients (n = 19)
Women/men	15/2	17/2
Age, years		
Mean ± SD	41 ± 12	45.7 ± 10
Range	20–57	27–64
Focus score†		
1	0	11
2	0	4
3	0	4
Unstimulated salivary flow rate, ml/15 minutes		
Mean ± SD	3.1 ± 1.2	1.4 ± 1.6‡
Range	0.8–5	0–4.5
Scintigraphic data score§		
1	13	0
2	4	6
3	0	13
Ro antibody positive	0	15
Ro/La antibody positive	0	9
ANA positive	0	17
RF positive	0	5

* Except where indicated otherwise, values are the number of subjects. SS = Sjögren's syndrome; ANA = antinuclear antibody; RF = rheumatoid factor.
† Number of foci/4 mm^2 of tissue.
‡ $P < 0.05$ versus controls.
§ Classified according to the method of Schall et al (21), where 1 = normal salivary gland function, 2 = mild to moderate impairment of salivary gland function, and 3 = severe to very severe impairment of salivary gland function.

Group criteria (20), and 17 subjects (age and sex matched) were classified as controls. Control subjects did not fulfill the primary SS classification criteria, were negative for rheumatoid factor, antinuclear antibody, and antibodies to Ro and La, and did not have systemic diseases. Analysis of lip biopsy specimens obtained from controls revealed nonfocal mild diffuse chronic sialadenitis. (Results are available from the author upon request.)

Evaluation of the salivary glands by scintigraphy was performed according to the method of Schall et al (21,22). Scintigraphy data from all patients were assigned a score of 1–3, where 1 = normal salivary gland function, 2 = mild to moderate impairment of salivary gland function, and 3 = severe to very severe impairment of salivary gland function (Table 1). To determine protein levels of GTPases, SS patients were grouped into 4 categories according to unstimulated salivary flow rate (low or normal) and focus score. Thus, the 4 subgroups analyzed were focus score of 1 and normal unstimulated salivary flow rate (mean ± SD rate 3.4 ± 1.2 ml/15 minutes; n = 6), focus score of 1 and low unstimulated salivary flow rate (mean ± SD rate 0.6 ± 0.5; n = 5), focus score of 2 and low unstimulated salivary flow rate (mean ± SD rate 0.8 ± 0.7; n = 4), and focus score of 3 and low unstimulated salivary flow rate (mean ± SD rate 0.2 ± 0.1; n = 4).

Biopsy specimens. LSG specimens were obtained as previously described (23). Following surgery, samples were split into 2 portions. One portion was immediately frozen in liquid nitrogen and stored at −80°C to extract RNA and proteins. The second portion was processed for morphologic characterization and immunofluorescence experiments.

Quantitative reverse transcriptase–polymerase chain reaction (PCR). RNA was extracted, and RNA yields and purity were evaluated essentially as previously described (24,25). The primer sequences for the genes h18S, Rab3D, and Rab8A were designed using the programs AmplifX, version 1.4, and Primer3, version 0.4.0. The forward and reverse primers, size of the PCR products, and melting and annealing temperatures were as follows: for h18S (236 bp), forward 5′-GATATGCTCATGTGGTGTTG-3′ and reverse 5′-AATCTTCTTCAGTCGCTCCA-3′, melting at 83.3°C and annealing at 60°C; for Rab3D (165 bp), forward 5′-TACTGTGGGCATCGATTTCA-3′ and reverse 5′-TCCTGATTGGCGATGTCATA-3′, melting at 85.3°C and annealing at 60°C; and for Rab8A (169 bp), forward 5′-AGAGCTCGATGGCAAGAGAA-3′ and reverse 5′-AATGTTGCGAATCCAGTTCC-3′, melting at 84.3°C and annealing at 60°C. For quantitative PCR, the Brilliant II SYBR Green Quantitative PCR Master Mix kit (Stratagene) was used. Template complementary DNA (cDNA) was obtained by reverse transcription of 3 μg of total RNA with SuperScript II reverse transcriptase (Invitrogen).

For amplification, 35 PCR cycles, consisting of denaturation at 95°C for 15 seconds, primer annealing at 46–65°C (depending on the primer pair) for 15 seconds, and elongation at 72°C for 15 seconds, were performed. Dissociation curves to determine the specificity and melting temperature of DNA amplicons were obtained using one additional cycle consisting of denaturation at 95°C for 10 seconds, hybridizing at 70°C for 1 second, and a gradual increase in increments of 0.02°C/second up to 95°C over 10 minutes. C_t values and efficiency were obtained from standard curves with a control sample using serial dilutions of the cDNA for all genes to be evaluated and a housekeeping gene (h18S). The relative expression ratio of a target gene was expressed in comparison to a reference gene using the formula described by Pfaffl (26) and REST 2008. Ratios >1.0 indicated up-regulation, and ratios <1.0 indicated down-regulation.

Protein extraction and Western blotting. Experiments were performed essentially as previously described (24). Briefly, LSG specimens were homogenized in radioimmunoprecipitation assay buffer (50 m*M* Tris, pH 8.0, 150 m*M* NaCl, 0.1% sodium dodecyl sulfate [SDS], 0.5% deoxycholate, and 1% Nonidet P40) containing protease inhibitors (4 m*M* phenylmethylsulfonyl fluoride, 10 μM leupeptin, and 2.8 μM aprotinin). Protein concentration was determined by the Bradford method (27). Proteins were resolved by SDS–polyacrylamide gel electrophoresis in 11% gels under reducing and denaturing conditions and then electrotransferred onto nitrocellulose membranes for 15 hours at 4°C. Membranes were blocked for 1 hour at room temperature in a 5% skim milk, protease-free solution prepared in TBST (10 m*M* Tris HCl, pH 7.5, 150 m*M* NaCl, 0.05% Tween 20). Blots were incubated separately with antibodies against Rab3D, Rab8A, and β-actin for 2 hours at room temperature. (A list of the antibodies used is available from the author upon request.) After 5 washes in TBST buffer, membranes were incubated with horseradish peroxidase–conjugated anti-mouse or anti-rabbit secondary antibodies (Jackson ImmunoResearch) for 1 hour at room temperature. Target proteins were immuno-

detected by chemiluminescence (SuperSignal West Pico chemiluminescent substrate). Protein bands were quantified by densitometry. Levels of proteins of interest were normalized to β-actin. The results reported were averaged from 3 sets of independent experiments.

Immunofluorescence analysis. LSG specimens were fixed in 1% paraformaldehyde and then embedded in paraffin. Sections were used to study Rab3D, Rab8A, MUC7, ezrin, EBP50, and TGN46 distribution (trans-Golgi network). Antigen detection was recovered by incubation with a 0.01*M* citrate solution (pH 6.0) for 25 minutes at 92°C. The sections were then blocked with 0.25% casein in phosphate buffered saline and incubated with primary antibodies, followed by Alexa Fluor 488–conjugated or Alexa Fluor 546–conjugated secondary antibodies. (A list of the antibodies used is available from the author upon request.) Staining was visualized with a confocal Zeiss microscope (model LSM-410 Axiovert 100). High-resolution digital images were captured and stored in TIFF format. As a negative control, rabbit Ig or mouse IgG1 fractions (DakoCytomation) were used.

Quantification of fluorescence of Rab3D and Rab8A in acinar cells. Confocal image stacks were captured with an Olympus FluoView 1000 confocal microscope. Two-channel fluorescent image stacks (intensity I[x,y,z], voxel size $\Delta x/\Delta y/\Delta z$ = 50/50/300 nm) were recorded in multitrack mode. Channel 1 (Alexa Fluor 488) was used with excitation and emission wavelengths λ_{ex} = 488 nm and λ_{em} = 520 nm, respectively, and channel 2 (Alexa Fluor 546) was used with λ_{ex} = 543 nm and λ_{em} = 572 nm. Adjustments in laser power, detector gain, and detector offset ensured that I(x,y,z) did not saturate and that the image background was slightly above 0. Image stacks were deconvolved with Huygens Professional/Scripting (from Scientific Volume Imaging). All image processing routines were developed in our laboratory using Interactive Data Language software (from ITT). To determine Rab3D and Rab8A distribution, apical and basal regions of interest (ROIs) were defined by segmentation. Artifacts were removed with morphologic filters. The quality of the final segmentation was controlled interactively by overlaying the images with the segmented ROI. The nuclear region was defined manually using the brightfield image and excluded from the ROI. Cytoplasmic fluorescence intensities were determined inside the apical and basal ROIs and divided by the respective areas ($I/\mu m^2$). Identical protocols were applied in all experiments.

Statistical analysis. The mean values in control and patient groups were compared using the Mann-Whitney test. Correlations of mRNA and protein levels with clinical covariates were established using Spearman's rank test and Pearson's test. *P* values less than 0.05 were considered significant.

RESULTS

Levels of Rab3D and Rab8A mRNA and protein. Previous studies have implicated Rab3D in the exocytosis of mature secretory granules localized at the apical

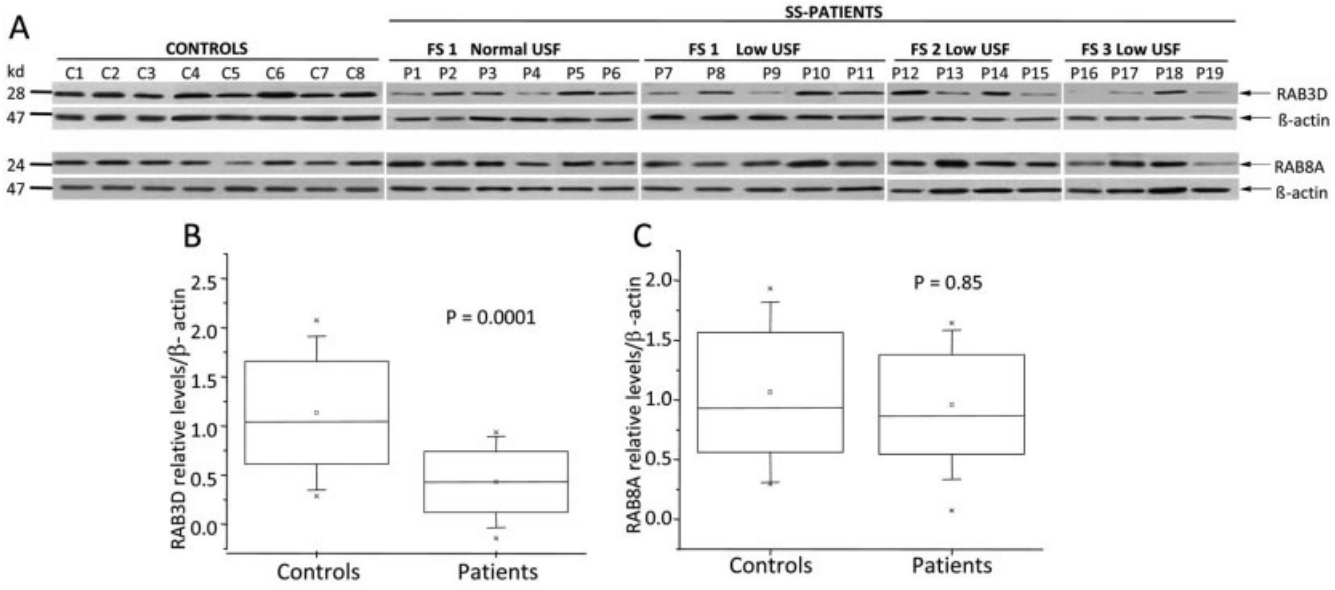

Figure 1. Rab3D and Rab8A protein levels in labial salivary gland (LSG) specimens from patients with Sjögren's syndrome (SS) classified by unstimulated salivary flow (USF) rate and focus score (FS). LSG protein extracts from controls and SS patients were subjected to Western blotting as described in Patients and Methods. **A,** Single immunoreactive bands for Rab3D (28 kd), Rab8A (24 kd), and β-actin (47 kd). **B** and **C,** Relative levels of Rab3D (**B**) and Rab8A (**C**) in LSG specimens from controls and patients, determined by ratiometric analysis of the densitometric data from all samples. Values were normalized to β-actin. Data are presented as box plots, where boxes represent the 25th to 75th percentiles, lines within the boxes represent the median, squares represent the mean, lines outside the boxes represent the standard deviation, and x's represent outliers. Results were averaged from data obtained in 3 independent experiments.

pole of acinar cells (16,17). In contrast, Rab8A has been detected in the basal region of epithelial cells (28–30). Therefore, in this study we assessed protein levels and levels of mRNA for these 2 GTPases in LSGs from 19 patients with SS and 17 control subjects. Levels of mRNA for Rab3D and Rab8A did not differ significantly between patients and controls ($P = 0.7$ and $P = 0.9$, respectively) (data not shown). Rab3D protein levels were significantly decreased in SS patients compared to controls ($P = 0.0001$), while no changes were observed for Rab8A ($P = 0.85$) (Figures 1A–C). The changes observed for Rab3D protein levels were not related to focus score. (Data are available from the author upon request.) A Spearman's correlation analysis comparing diverse clinical parameters with Rab3D and Rab8A protein and mRNA levels revealed a moderate to strong inverse correlation between Rab3D protein level and glandular function measured by scintigraphy ($r = -0.5123$, $P = 0.0249$) and between Rab3D mRNA level and glandular function measured by scintigraphy ($r = -0.8729$, $P = 0.0047$).

Localization and subcellular distribution of Rab3D in serous acinar cells. Efficient exocytosis requires that Rab3D be associated with secretory granules. Thus, Rab3D distribution was assayed by immunofluorescence analysis and confocal microscopy. The serous acini of LSG specimens from SS patients showed the following 4 patterns of Rab3D staining: severely decreased staining (10% of acini) (Figures 2C and D), distribution of staining throughout the cytoplasm (50% of acini) (Figures 2E and F), distribution of staining throughout the cytoplasm that was paralleled by loss of nuclear polarity (10% of acini) (Figures 2G and H), and staining similar to that seen in controls (30% of acini) (Figures 2A and B). The observed changes were independent of their proximity to inflammatory cell infiltrates. (Results are available from the author upon request.) In contrast, staining of mucous acini for Rab3D was similar in both SS patient and control groups (results not shown).

Localization of Rab3D relative to apical and basal subcellular markers of cell polarity. Rab8A was used as a basal marker, ezrin was used as an apical marker, and TGN46 was used as a Golgi complex marker. Figures 3A, C, E, and G show photomicrographs of acini from controls, and Figures 3B, D, F, and H show photomicrographs of acini from SS patients. In controls, Rab3D was found only in apical structures, and Rab8A was found only in basal structures (Figure 3A). In the acini of SS patients, Rab3D was found throughout the cytoplasm, while Rab8A localization remained unaltered (Figure 3B). This observation was confirmed by

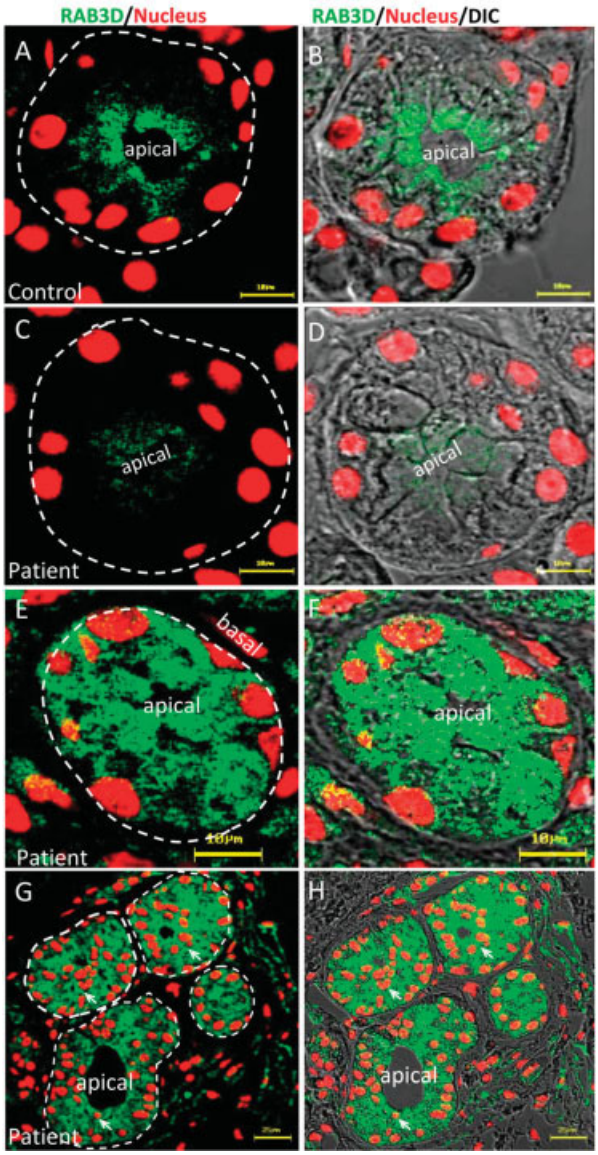

Figure 2. Rab3D immunolocalization and subcellular distribution in acinar cells from controls and patients with Sjögren's syndrome (SS). Selected control and SS patient samples were processed as described in Patients and Methods. Samples were stained for Rab3D (green) and nuclei (red). **A, C, E,** and **G,** Representative immunofluorescence images of a control subject sample (**A**), an SS patient sample with strongly decreased Rab3D staining (**C**), an SS patient sample with Rab3D distribution throughout the cytoplasm (**E**), and an SS patient sample with Rab3D distribution throughout the cytoplasm and additional loss of nuclear polarity (**arrows**) (**G**). Broken lines indicate the edges of acini. **B, D, F,** and **H,** Overlap of the immunofluorescence images shown in **A, C, E,** and **G** with differential interference contrast (DIC) images of a control subject sample (**B**), an SS patient sample with strongly decreased Rab3D staining (**D**), an SS patient sample with Rab3D distribution throughout the cytoplasm (**F**), and an SS patient sample with Rab3D distribution throughout the cytoplasm and additional loss of nuclear polarity (**arrows**) (**H**). Bars in **A–F** = 10 μm; bars in **G** and **H** = 25 μm.

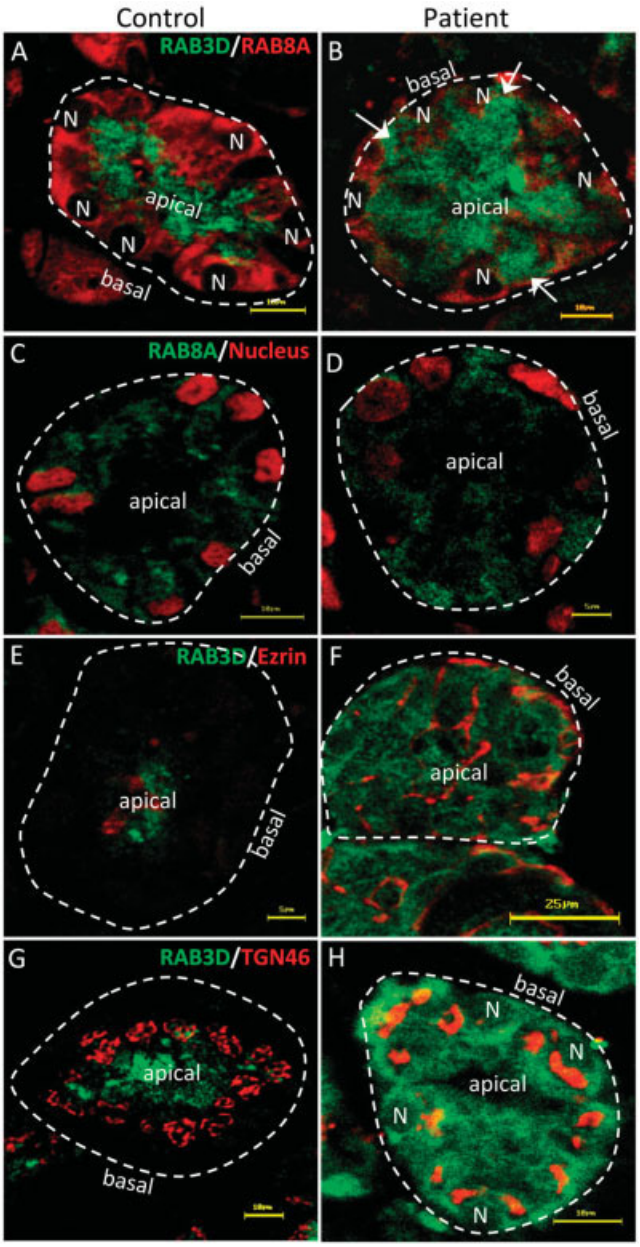

Figure 3. Rab3D immunolocalization relative to apical and basal subcellular markers of cell polarity. Selected samples from control subjects and patients with Sjögren's syndrome (SS) were processed as described in Patients and Methods. Rab8A was used as a basal marker, ezrin was used as an apical marker, and TGN46 was used as a Golgi complex marker. **A, C, E,** and **G,** Representative samples from control subjects showing staining for Rab3D (green) and nuclei (**N**; red) (**A**), Rab8a (green) and nuclei (red) (**C**), Rab3D (green) and ezrin (red) (**E**), and Rab3D (green) and TGN46 (red) (**G**). **B, D, F,** and **H,** Representative samples from SS patients showing staining for Rab3D (green) and nuclei (red) (**B**), Rab8A (green) and nuclei (red) (**D**), Rab3D (green) and ezrin (red) (**F**), and Rab3D (green) and TGN46 (red) (**H**). Broken lines indicate the edges of acini; **arrows** indicate Rab3D in the basal cytoplasm. Bars in **A, B, C, E, F, G,** and **H** = 10 μm; bars in **D** = 5 μm.

staining for Rab8A and nuclei, which showed that Rab8A retained its basal localization relative to the nucleus in both groups (Figures 3C and D). Apical localization of ezrin, a microvilli-associated protein, was observed in controls, while ezrin also localized in basal compartments in acini from SS patients (Figures 3E and F). In acini from controls, Golgi stacks (TGN46) were characteristically detected in apical regions of the Golgi complex next to Rab3D-positive secretory granules. Supranuclear localization of TGN46 was not altered in acini from SS patients, but thicker Golgi stacks were

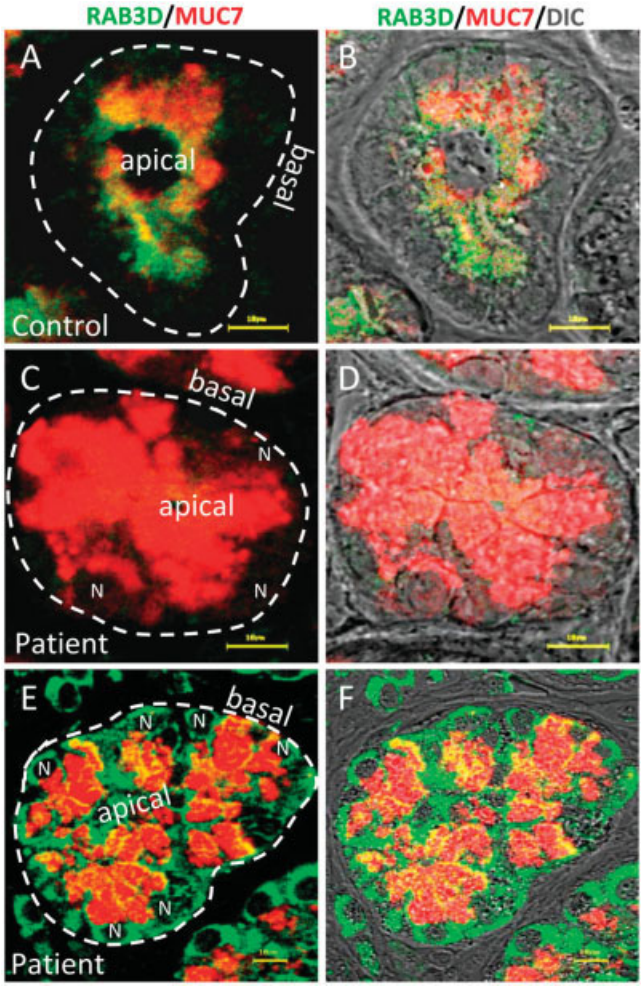

Figure 4. Simultaneous localization of Rab3D and secretory mucin in acini. **A** and **B,** Acini from a control subject with both Rab3D (green) and mucin 7 (MUC7) (red) localized in the apical cytoplasm. **C** and **D,** Acini from a patient with Sjögren's syndrome (SS) with very low staining for Rab3D and pronounced MUC7 accumulation in the cytoplasm. **E** and **F,** Acini from an SS patient with Rab3D distributed throughout the cytoplasm and cytoplasmic accumulation of MUC7. Bars = 10 μm. DIC = differential interference contrast; **N** = nucleus.

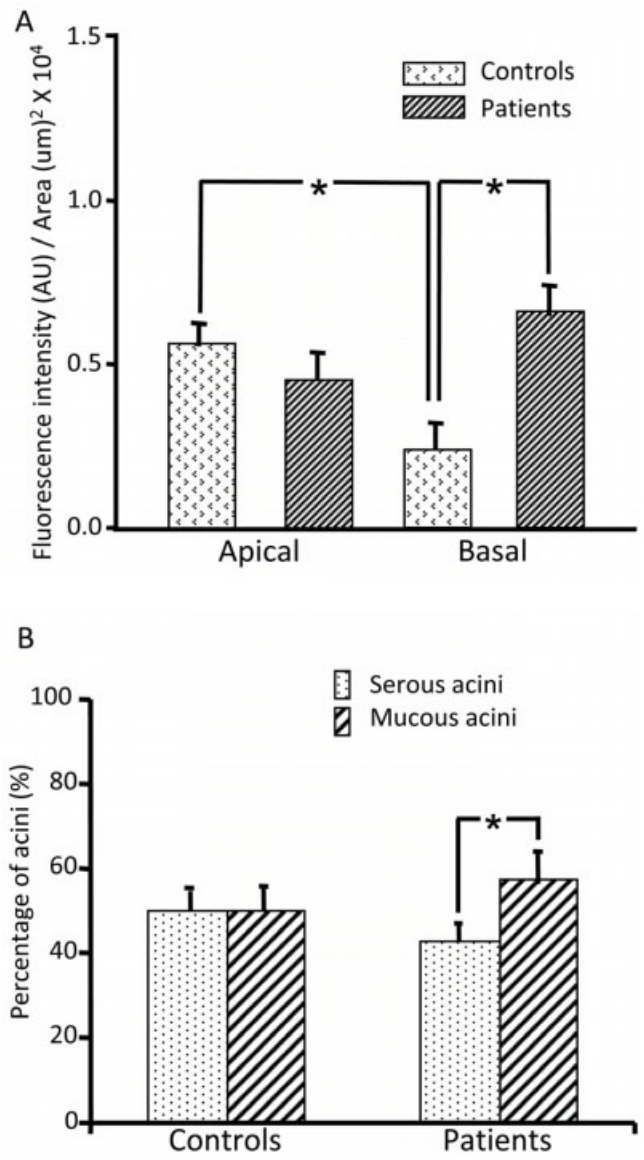

Figure 5. Discrepancy between total Rab3D protein levels in glandular extracts and Rab3D expression in acini. **A,** Fluorescence intensity of Rab3D in apical and basal regions of acini samples from controls and patients with Sjögren's syndrome (SS). Rab3D-specific fluorescence in serous acinar cells revealed the presence of Rab3D throughout the cytoplasm with stronger staining in the basal region of acini from SS patients than controls. $* = P < 0.05$. AU = arbitrary units. **B,** Percentages of serous acini and mucous acini in controls and SS patients. The number of serous acini was significantly lower than the number of mucous acini in SS patients. $* = P = 0.006$.

observed in those acini in which Rab3D was distributed throughout the cytoplasm (Figures 3G and H).

Simultaneous localization of Rab3D and secretory mucin in serous acini. MUC7 is a mucin that is synthesized by serous acini. To assess whether the changes described for Rab3D expression and localization were related to secretion, Rab3D and MUC7 distribution were analyzed simultaneously. In controls, MUC7 was detected predominantly in the apical region of acinar cells and colocalized there with Rab3D (Figures 4A and B). In contrast, pronounced MUC7 accumulation in the cytoplasm was observed in both acini from SS patients expressing low Rab3D levels (Figures 4C and D) and acini from SS patients expressing high Rab3D levels (Figures 4E and F).

Discrepancy between total Rab3D protein levels in glandular extracts and Rab3D expression in acini. As described above, Rab3D total protein levels were significantly decreased in glandular extracts from SS patients. However, in ~50% of serous acini from SS patients, intense Rab3D staining throughout the cytoplasm was visible. To shed light on this apparent discrepancy, two approaches were used. First, the fluorescence intensity of serous acini with cytosolic Rab3D was quantified. Cytoplasmic fluorescence intensity was determined in the apical and basal regions of serous acinar cells and divided by the respective surface areas ($I/\mu m^2$). In controls, the fluorescence signal was significantly higher in the apical region than in the basal region. No differences were observed between the apical region in controls and the apical region in SS patients, while the signal in the basal region was significantly stronger in SS patients than in controls (Figure 5A). Second, to explain the decrease in Rab3D protein levels in glandular extracts, the numbers of serous and mucous acini were quantified. Two independent observers (VB and CA) identified serous and mucous acini in a double-blind analysis of a total of 6,038 randomly selected acini (2,842 acini from 11 LSG specimens from controls and 3,196 acini from 14 LSG specimens from patients). As shown in Figure 5B, the number of serous acini in SS patients was significantly lower than the number of mucous acini ($P = 0.006$).

DISCUSSION

The amount of residual LSG parenchyma in SS patients does not necessarily reflect its functionality. Patients with a focus score of 1 and either normal or low unstimulated salivary flow rates showed decreased protein Rab3D levels in glandular extracts (Figure 1). The lack of correlation between Rab3D protein levels and unstimulated salivary flow rate demonstrates that the exocytotic pathway involving secretory granules and Rab3D is not necessarily related to the pathway implicated in the release of water and electrolytes. This finding should be taken into account in current xero-

stomia therapies, which are mostly focused on improving the aqueous content of saliva. Additionally, the population of LSG serous acini in these patients showed a mosaic expression pattern for Rab3D, where the amount and distribution of Rab3D varied among acini (Figure 2).

SS patients with higher focus scores exhibited the same tendency as those with low focus scores, i.e., decreased Rab3D protein levels in glandular extracts and a mosaic pattern of Rab3D expression. Rab3D mRNA levels, measured in total RNA isolated from LSG extracts, were similar in SS patients and controls ($P = 0.7$). However, for ~50% of the acini, protein levels actually increased. In these cases, we cannot rule out the possibility that higher Rab3D protein expression may also correlate with elevated mRNA levels. Then again, recent proteomic studies indicate that only 50% or fewer of the observed variations in protein abundance can be attributed to variations in mRNA levels (31). With this in mind, it is perhaps not particularly relevant whether alterations in Rab3D mRNA levels were observed or not.

However, no apparent changes in the expression of Rab3D were detectable in mucous acini. Thus, in SS patients the number of serous acini decreased relative to the number of mucous acini. This decrease in serous acini may be the consequence of cell death by anoikis in those acini where nuclear polarity was lost and Rab3D distribution throughout the cytoplasm was observed. Interestingly, Rab8A was not affected, indicating that the changes in Rab3D in SS patients were specific to this isoform and not a generic alteration observed for all Rabs.

Given that Rab3D plays a prevalent role in apical exocytosis, our observations suggest that this process is likely to be altered. Experiments comparing the distribution of Rab3D and MUC7, a mucin secreted by serous acini, revealed MUC7 accumulation in acini from SS patients compared to controls (Figure 4). These observations corroborate the notion that a lack of Rab3D affects the fusion of granules with the plasma membrane. However, it should be noted that for acini with increased Rab3D expression throughout the cytoplasm, high local expression of MUC7 was also detected. This accumulation of secretory granules positive for Rab3D and MUC7 has two possible, yet contradictory, explanations. The accumulation may be caused by an increase in the biogenesis of secretory granules. Alternatively, it may be caused by altered trafficking and granule accumulation localized in subcellular regions where other components of the exocytotic machinery (i.e., soluble N-ethylmaleimide–sensitive factor attachment protein receptors [SNAREs]) do not promote exocytosis. Preliminary studies from our laboratory indicate that the localization of SNARE proteins is altered at the plasma membrane. Moreover, levels of secretory granule SNARE proteins are increased. In the latter case, granule–granule fusion events occur, as suggested by our previous studies, which identified large, pleomorphic secretory granules in LSGs from SS patients (10).

Interestingly, da Costa et al observed the formation of irregularly shaped, unusually large secretory vesicles in lacrimal glands from NOD mice (19). Depending on the age of the mice, Rab3D distribution throughout the cytoplasm was also observed. However, in contrast to our findings, they did not report changes in Rab3D protein levels in gland extracts (19). Moreover, increased amounts of Rab3D on membranes of von Willebrand factor (vWF) granules have been shown to result in a marked inhibition of the Ca^{2+}-regulated exocytosis of these granules (32). Such inhibition may reflect direct inhibitory effects of Rab3D on later steps of exocytosis, or increased recruitment of Rab3D effectors required for vWF granule maturation/fusion that adversely affect exocytotic fusion with the plasma membrane (32). Either of these explanations may account for the increase in Rab3D observed throughout the cytoplasm of acini from SS patients.

Additionally, studies using Rab3D-knockout mice have provided evidence for a role of Rab3D in the maturation and/or maintenance of secretory granules (33). In this mouse model, secretory granules from pancreatic and parotid acinar cells were increased in size, consistent with the notion that Rab3D acts as an inhibitor of granule–granule fusion in exocrine glands (33). As mentioned above, secretory granules of large size and pleomorphic shape have been observed in the majority of acini from LSGs of SS patients (10). In the present study, we identified 4 different Rab3D expression patterns in a single gland. Therefore, this observation is not consistent with findings in the Rab3D-knockout mouse model, particularly in those acini showing high Rab3D expression. The increased size of secretory granules could be related to low levels of sulfated mucins that have been demonstrated in the LSGs of SS patients, which is not related to the saliva volume (8). Sulfated and sialic acid residues interact with Ca^{2+} and H^+, generating interstrand crosslinks that displace water molecules and compact the mucin granule (34,35). Thus, low sulfation of mucins will unfavorably impact secretory granule assembly.

Posttranslational processing of mucins, including *O*-glycosylation, *N*-glycosylation, and sulfation, occur in the Golgi complex, which was found to be enlarged in SS

patients (Figure 3H). The size and structure of trans-Golgi network (TGN) stacks depend on the amounts of exocytotic and endocytotic cargo this organelle is carrying (36–38). The biogenesis of secretory granules occurs in the TGN. Under physiologic conditions, these stacks are small in size, as was observed for acinar cells from control subjects (38). Conversely, TGN "hypertrophy" has been observed under two conditions: pharmacologic conditions which chronically stimulate secretory cells (38) and lysosome accumulation diseases (39). Thus, the Golgi complex could be the organelle involved in the changes observed in this study. Further studies are necessary to shed light on these alterations in Golgi complex morphology.

Recently, we have reported on the loss of acinar cell polarity, modifications in tight junction proteins, and acinar cell–extracellular matrix interactions (7,10,11). These changes, in addition to relocalization of ezrin and actin from apical to basal membranes, could alter the directionality of the secretory pathway and eventually promote accumulation of Rab3D-positive secretory granules in basolateral regions, as well as ectopic basolateral exocytosis. If components of secretory granules are transferred to the extracellular matrix by exocytosis, a local inflammatory response would likely be the consequence. Experiments to address this interesting aspect are currently being developed in our laboratory.

Rab3D is a key GTPase involved in the secretory pathway controlling saliva composition, not linked to water content but associated with the levels of other components that are critical in the maintenance of oral physiology. This study is the first to identify specific changes in the expression and distribution of Rab3D, but not Rab8A, in SS patients. The decrease in or loss of saliva components as a consequence of the observed changes in Rab3D might explain the multiple, often heterogeneous, patterns of oral symptoms that SS patients experience. This study provides new insights into the pathogenesis of SS that are helpful in developing an understanding of how alterations in the secretion of saliva components, other than water and electrolytes, occur. These findings may lead to the identification of new targets for therapeutic interventions.

ACKNOWLEDGMENTS

The authors thank Alejandra García and Uwe Schubmehl from SCIAN-Lab (www.scian.cl) for their help in image processing and the quantification of immunofluorescence data.

AUTHOR CONTRIBUTIONS

All authors were involved in drafting the article or revising it critically for important intellectual content, and all authors approved the final version to be published. Dr González had full access to all of the data in the study and takes responsibility for the integrity of the data and the accuracy of the data analysis.

Study conception and design. Bahamondes, Aguilera, Alliende, Molina, Castro, M-J González.

Acquisition of data. Bahamondes, Albornoz, Aguilera, Alliende, Barrera, S. González, Sánchez, Härtel, Hermoso, Leyton.

Analysis and interpretation of data. Bahamondes, Aguilera, Alliende, Molina, Urzúa, Quest, Härtel, M-J González.

REFERENCES

1. Alpert S, Kang HI, Weissman I, Fox RI. Expression of granzyme A in salivary gland biopsies from patients with primary Sjögren's syndrome. Arthritis Rheum 1994;37:1046–54.
2. Manganelli P, Fietta P. Apoptosis and Sjögren syndrome. Semin Arthritis Rheum 2003;33:49–65.
3. Ramos-Casals M, Font J. Primary Sjögren's syndrome: current and emergent aetiopathogenic concepts. Rheumatology (Oxford) 2005;44:1354–67.
4. Dawson LJ, Fox PC, Smith PM. Sjögren's syndrome—the non-apoptotic model of glandular hypofunction. Rheumatology (Oxford) 2006;45:792–8.
5. Dawson LJ, Field EA, Harmer AR, Smith PM. Acetylcholine-evoked calcium mobilization and ion channel activation in human labial gland acinar cells from patients with primary Sjögren's syndrome. Clin Exp Immunol 2001;124:480–5.
6. Fox RI. Sjögren's syndrome. Lancet 2005;366:321–31.
7. Ewert P, Aguilera S, Alliende C, Kwon YJ, Albornoz A, Molina C, et al. Disruption of tight junction structure in salivary glands from Sjögren's syndrome patients is linked to proinflammatory cytokine exposure. Arthritis Rheum 2010;62:1280–9.
8. Alliende C, Kwon YJ, Brito M, Molina C, Aguilera S, Perez P, et al. Reduced sulfation of muc5b is linked to xerostomia in patients with Sjögren syndrome. Ann Rheum Dis 2008;67:1480–7.
9. Thomsson KA, Prakobphol A, Leffler H, Reddy MS, Levine MJ, Fisher SJ, et al. The salivary mucin MG1 (MUC5B) carries a repertoire of unique oligosaccharides that is large and diverse. Glycobiology 2002;12:1–14.
10. Goicovich E, Molina C, Perez P, Aguilera S, Fernandez J, Olea N, et al. Enhanced degradation of proteins of the basal lamina and stroma by matrix metalloproteinases from the salivary glands of Sjögren's syndrome patients: correlation with reduced structural integrity of acini and ducts. Arthritis Rheum 2003;48:2573–84.
11. Perez P, Aguilera S, Olea N, Alliende C, Molina C, Brito M, et al. Aberrant localization of ezrin correlates with salivary acini disorganization in Sjögren's syndrome. Rheumatology (Oxford) 2010; 49:915–23.
12. Grosshans BL, Ortiz D, Novick P. Rabs and their effectors: achieving specificity in membrane traffic. Proc Natl Acad Sci U S A 2006;103:11821–7.
13. Takai Y, Sasaki T, Matozaki T. Small GTP-binding proteins. Physiol Rev 2001;81:153–208.
14. Seabra MC, Mules EH, Hume AN. Rab GTPases, intracellular traffic and disease. Trends Mol Med 2002;8:23–30.
15. Schluter OM, Khvotchev M, Jahn R, Sudhof TC. Localization versus function of Rab3 proteins: evidence for a common regulatory role in controlling fusion. J Biol Chem 2002;277:40919–29.
16. Ohnishi H, Ernst SA, Wys N, McNiven M, Williams JA. Rab3D localizes to zymogen granules in rat pancreatic acini and other exocrine glands. Am J Physiol 1996;271:G531–8.
17. Raffaniello RD, Lin J, Schwimmer R, Ojakian GK. Expression

and localization of Rab3D in rat parotid gland. Biochim Biophys Acta 1999;1450:352–63.
18. Chen X, Edwards JA, Logsdon CD, Ernst SA, Williams JA. Dominant negative Rab3D inhibits amylase release from mouse pancreatic acini. J Biol Chem 2002;277:18002–9.
19. Da Costa SR, Wu K, Veigh MM, Pidgeon M, Ding C, Schechter JE, et al. Male NOD mouse external lacrimal glands exhibit profound changes in the exocytotic pathway early in postnatal development. Exp Eye Res 2006;82:33–45.
20. Vitali C, Bombardieri S, Jonsson R, Moutsopoulos HM, Alexander EL, Carsons SE, et al, and the European Study Group on Classification Criteria for Sjögren's Syndrome. Classification criteria for Sjögren's syndrome: a revised version of the European criteria proposed by the American-European Consensus Group. Ann Rheum Dis 2002;61:554–8.
21. Schall GL, Anderson LG, Wolf RO, Herdt JR, Tarpley TM Jr, Cummings NA, et al. Xerostomia in Sjögren's syndrome: evaluation by sequential salivary scintigraphy. JAMA 1971;216:2109–16.
22. Vinagre F, Santos MJ, Prata A, da Silva JC, Santos AI. Assessment of salivary gland function in Sjögren's syndrome: the role of salivary gland scintigraphy. Autoimmun Rev 2009;8:672–6.
23. Daniels TE. Labial salivary gland biopsy in Sjögren's syndrome: assessment as a diagnostic criterion in 362 suspected cases. Arthritis Rheum 1984;27:147–56.
24. Kwon YJ, Perez P, Aguilera S, Molina C, Leyton L, Alliende C, et al. Involvement of specific laminins and nidogens in the active remodeling of the basal lamina of labial salivary glands from patients with Sjögren's syndrome. Arthritis Rheum 2006;54:3465–75.
25. Perez P, Kwon YJ, Alliende C, Leyton L, Aguilera S, Molina C, et al. Increased acinar damage of salivary glands of patients with Sjögren's syndrome is paralleled by simultaneous imbalance of matrix metalloproteinase 3/tissue inhibitor of metalloproteinases 1 and matrix metalloproteinase 9/tissue inhibitor of metalloproteinases 1 ratios. Arthritis Rheum 2005;52:2751–60.
26. Pfaffl MW. A new mathematical model for relative quantification in real-time RT-PCR. Nucleic Acids Res 2001;29:e45.
27. Bradford MM. A rapid and sensitive method for the quantitation of microgram quantities of protein utilizing the principle of protein-dye binding. Anal Biochem 1976;72:248–54.
28. Henry L, Sheff DR. Rab8 regulates basolateral secretory, but not recycling, traffic at the recycling endosome. Mol Biol Cell 2008;19:2059–68.
29. Huber LA, Pimplikar S, Parton RG, Virta H, Zerial M, Simons K. Rab8, a small GTPase involved in vesicular traffic between the TGN and the basolateral plasma membrane. J Cell Biol 1993;123:35–45.
30. Peranen J, Auvinen P, Virta H, Wepf R, Simons K. Rab8 promotes polarized membrane transport through reorganization of actin and microtubules in fibroblasts. J Cell Biol 1996;135:153–67.
31. De Sousa Abreu R, Penalva LO, Marcotte EM, Vogel C. Global signatures of protein and mRNA expression levels. Mol Biosyst 2009;5:1512–26.
32. Knop M, Aareskjold E, Bode G, Gerke V. Rab3D and annexin A2 play a role in regulated secretion of vWF, but not tPA, from endothelial cells. EMBO J 2004;23:2982–92.
33. Riedel D, Antonin W, Fernandez-Chacon R, Alvarez de Toledo G, Jo T, Geppert M, et al. Rab3D is not required for exocrine exocytosis but for maintenance of normally sized secretory granules. Mol Cell Biol 2002;22:6487–97.
34. Espinosa M, Noe G, Troncoso C, Ho SB, Villalon M. Acidic pH and increasing [Ca^{2+}] reduce the swelling of mucins in primary cultures of human cervical cells. Hum Reprod 2002;17:1964–72.
35. Perez-Vilar J. Mucin granule intraluminal organization. Am J Respir Cell Mol Biol 2007;36:183–90.
36. De Matteis MA, Luini A. Exiting the Golgi complex. Nat Rev Mol Cell Biol 2008;9:273–84.
37. Griffiths G, Fuller SD, Back R, Hollinshead M, Pfeiffer S, Simons K. The dynamic nature of the Golgi complex. J Cell Biol 1989;108:277–97.
38. Hand AR, Oliver C. Effects of secretory stimulation on the Golgi apparatus and GERL of rat parotid acinar cells. J Histochem Cytochem 1984;32:403–12.
39. Vitry S, Bruyere J, Hocquemiller M, Bigou S, Ausseil J, Colle MA, et al. Storage vesicles in neurons are related to Golgi complex alterations in mucopolysaccharidosis IIIB. Am J Pathol 2010;177:2984–99.